International Journal of Energy Production and Management
https://www.acadlore.com/journals/IJEPM

Evaluation of Pore Space Conversion in Clayey Limestones upon Hydrogen-Methane Mixture Injection

Elisaveta A. Safarova[1*], Maria O. Sakharova[1], Anastasia K. Yumasheva[1], Iliya V. Malevin[2]

[1] Oil and Gas Research Institute, Russian Academy of Sciences, 119333 Moscow, Russia
[2] National University of Oil and Gas, Gubkin University, 119991 Moscow, Russia

[*] Correspondence: Elisaveta A. Safarova (safarova@ipng.ru)

Received: 10-18-2025 **Revised:** 12-01-2025 **Accepted:** 12-11-2025

Citation: E. A. Safarova, M. O. Sakharova, A. K. Yumasheva, I. V. Malevin, "Evaluation of pore space conversion in clayey limestones upon hydrogen-methane mixture injection," *Int. J. Energy Prod. Manag.*, vol. 10, no. 4, pp. 634–644, 2025. https://doi.org/10.56578/ijepm100405.

Abstract: As part of the study of the possibilities of using hydrogen as an alternative energy source, in particular in aspects of its underground storage, it is necessary to evaluate its interaction with host rocks. This article describes the initial results of experimental studies on carbonate rocks, specifically clayey limestones, when injecting hydrogen together with methane under given reservoir conditions typical for underground gas storage facilities, paying special attention to the assessment of changes in the pore space. The paper compares the method of computed tomography, which analyzes discrepancies in the attenuation of X-ray radiation by various rock components, and nuclear magnetic resonance relaxation, based on the phenomenon of resonant absorption of electromagnetic field energy by matter caused by nuclear paramagnetism. As a result of the interpretation of the analysis, it was shown that the overall and effective porosity remain stable as the values decreased for the tested samples by 0.1%, which indicates that hydrogen does not significantly affect the reservoir properties. An important result was the assessment of clay porosity, according to nuclear magnetic resonance relaxation calculations, its value increased by 2 times (from 0.15% to 0.28%) after exposure in the hydrogen-methane mixture, indicating the need to control the state of the overlapping clay strata and their integrity. These initial studies can be used in oil and gas field practice.

Keywords: Hydrogen-methane mixtures; Limestone; Pore structure; Porosity; Underground storage

1 Introduction

Hydrogen storage, including underground, is an essential part of the technological process of producing and using hydrogen as an energy source; therefore, ensuring the technical reliability and environmental safety of underground hydrogen storage (separately or together with methane) is highly relevant. The benefits of developing hydrogen energy have been recognized by many countries, regardless of the country's own resource potential. Projects on temporary hydrogen content in the bowels of the Earth are being successfully implemented, like HyUnder, H2STORE, SUN.STORAGE, and Hychico, etc. [1, 2]. For example, one of them provides seasonal placement of billions of cubic meters of hydrogen in natural conditions in geological formations in the UK [1]. As the volume of hydrogen produced increases, interest in its storage in geological reservoirs increases, whose capacities significantly exceed those of all types of terrestrial hydrogen storage facilities. It is assumed that by 2050, about 30% of technically produced hydrogen will be stored in underground reservoirs in its pure form or together with other gases [3].

Underground storage of hydrogen (USH) in geological formations is justified by the need to develop approaches for long-term, large-scale energy storage. At the same time, the development of USH technologies faces problems associated with diffusion losses, the potential risks of active geochemical reactions between hydrogen and reservoir rocks, as a result, the possible transformation of the reservoir and mechanical properties of the host and overlapping strata [4, 5]. The active reactivity of hydrogen in contact with host rocks and caprocks of an underground gas storage facility may be accompanied by the dissolution of rock-forming minerals or the precipitation of salts from an aqueous solution, i.e., secondary mineral formation [6–8]. Hydrogen reacts most actively with rock-forming minerals, in which the content of calcium, magnesium, sulfur, and iron is increased [9].

The solubility of hydrogen in reservoir fluids changes the pH of the medium and the geochemical equilibrium and activates redox reactions. This can change the permeability and porosity of the medium [10], as well as affect

the performance, safety, and stability of the host medium. As a result of such reactions, the alkaline properties of the medium are enhanced, which is often accompanied by the precipitation of insoluble precipitates (for example, calcium carbonates and sulfates, iron sulfides, etc.) and changes in the filtration properties of the pore space of reservoirs. Carbonate minerals are strongly affected by hydrogen injection. It has been described in the existing literature that carbonate and sulfate minerals such as calcite, dolomite, siderite, gypsum, anhydrite, and barite, as well as feldspar and clay minerals of the chlorite group, can undergo dissolution under PV conditions [11–13]. Based on the analysis of published scientific studies and theoretical ideas about the effect of hydrogen on various groups of sedimentary rock minerals, the main potential reaction agents are identified: calcite ($CaCO_3^{2-}$), aluminosilicates (the gross formula $H_4Al_2O_9Si_2 * 2H_2O$), sulfates (SO_4^{2-}), silicates (the gross formula SiO_4), oxides (Fe_2O_3), and iron sulfides (FeS). The main mineral associations provide the internal properties of the rock, such as structure and texture, which, if significantly changed, can have a negative impact on the mechanical storage tanks [7]. It is important to note that the reaction products caused by the initial change in the rock can have a negative impact on both the host layer and the composition of the stored gas [14, 15].

Heinemann et al. [16] found that in low-mineralized waters, carbonic acid salts and molecular hydrogen can react to form methane and a hydroxyl group:

- Reaction with calcite: $CaCO_3 + 4H_2 \rightarrow Ca^{2+} + CH_4 + 2OH^- + H_2O$
- Reaction with dolomite: $CaMg\,(CO_3)^2 + 8H_2 \rightarrow Ca^{2+} + Mg^{2+} + 2CH_4 + 4OH^- + 2H_2O$

The above processes are associated with subsequent risks of changes in the ratio of components of the gas mixture and the development of corrosion effects. The scale of these processes is large: almost all lithological types of storage facilities are subject to technogenically caused epigenesis caused by the violation of natural geochemical, hydrochemical, and microbiological conditions of the geological environment. The experience of storing hydrogen-methane mixtures (HMM) in geological structures is very limited; the available knowledge on the impact of $H_2 - CH_4$ mixture on the petrophysical properties of storage rocks shows limited influence on the properties of the rock [17]. The use of hybrid gas mixtures, such as hydrogen together with methane, is predetermined by the technical and economic agenda and is due to the need to fulfill the European Union climate goals declared for 2030 [18].

The existing tests of the gas infrastructure served as the basis for studying the reactivity of the gas mixture of $H_2 - 20\%$ and $CH_4 - 80\%$ [19]. The objective of this research was to evaluate changes in the pore space and porosity of clayey limestones after exposure to HMM under reservoir conditions. The research was motivated by the limited understanding of how HMM affect the pore structure and integrity of clayey limestone reservoirs during underground storage. It is possible to compare the pore sizes of different samples by considering the temporal variation of the NMR signal amplitude, as shown in Figure 1.

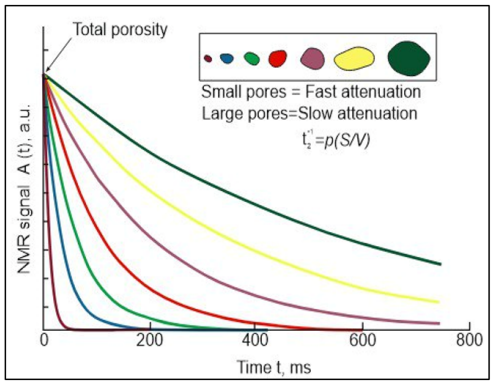

Figure 1. NMR signal from pores of various sizes [20]

The novelty lies in combining Computer tomography (CT) and NMR methods to monitor microstructural transformations in clayey limestones due to hydrogen-methane interactions. The result of NMR studies in the field of permanent magnets is a signal distribution spectrum over transverse relaxation times in the range from units to thousands of milliseconds. Mathematical processing of the spectrum allows us to obtain the following parameters: coefficient of total porosity, Kp, clay porosity, Kp_{cl}, capillary-bound water porosity, Kp_{cbw}, and effective porosity, Kp_{eff}.

It is found that the slower the signal attenuation, the larger the pore size. In order to estimate the overall trend of the signal, it was averaged. Thus, it is possible to approximately compare the pore size before and after exposure in hydrogen-methane mixtures.

The slower the signal attenuation, the larger the pore size. Signal averaging was performed to estimate the overall trend. Thus, it is possible to approximately compare the pore size before and after exposure to hydrogen-methane mixtures.

2 Methodology

As part of studies to assess the degree of transformation of the reservoir properties of carbonate rocks when interacting with hydrogen-methane mixtures, experimental work was carried out on core material. Addressing this issue requires an integrated approach and leads to the development of a unified core analysis methodology. Experimental work was carried out on Lower Permian clayey limestones, sampling depth 3820–3840 m. The core was placed in an autoclave for 2.5 months with an injected hydrogen-methane mixture. The technical characteristics of the experiment are presented in Table 1.

Table 1. Technical specifications of the autoclave and the object of study

Title	Value
The object	Clayey limestones
Core size and shape	Cylindrical shape $30^{*}30$ mm
Operating pressure and temperature	Pressure 8 MPa , temperature 24°C
The component composition of the gas mixture	$20\% - H_2, 80\% - CH_4$
Exposure period	2.5 months
Autoclave material	12X18H10T stainless steel (AISI 321)

CT, infrared spectroscopy (IR), and nuclear magnetic resonance (NMR) methods were used to monitor changes in the test system. The entire complex of analytical work was performed on samples both before and after the experiment, as shown in Figure 2. Pairs of twin samples of 30 mm were selected from a single interval of the full-size core (10 mm) and compared using a macro tomograph. Then, before placing it in a high-pressure vessel, CT and IR spectroscopy were performed. The NMR method involves comparing twin pairs, which requires sample heating, as per the analysis methodology. After that, the core was placed in a vessel (autoclave), pre-evacuated, into which the test gas mixture was supplied at a pressure of 8 MPa and a temperature of 24 ℃. The autoclave is made of corrosion-resistant steel with gaskets made of the same material, manufactured according to GOST P53561-2009. After the HMM exposure interval had expired, the core was extracted and reanalyzed using CT, IR, and NMR methods.

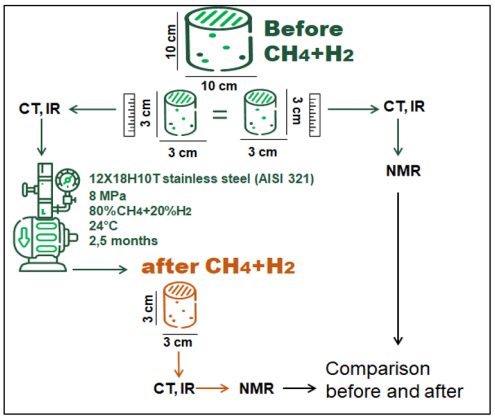

Figure 2. Flowchart of the experimental procedure

Fourier transform IR of the samples was performed at room temperature using a WQF-530A IR spectrometer (BEIJING RAYLEIGH ANALYTICAL INSTRUMENT CORP) with a Quest Single Reflection (ATR) accessory. All spectra were obtained using 32 scans with a resolution of 4 cm^{-1} in the wavelength range of 500–4,000 cm^{-1}. The core samples were analyzed using a NMR relaxometer Bruker Minispec mq10 NMR relaxometer. The temperature in the measuring area of the relaxometer is maintained at 40 ℃; therefore, for the correct conduct of the experiment, the samples were heated in a thermostat at 40 ℃ for two hours. After that, the samples were placed in the measuring area of the device in a special glass capsule. To obtain T2 distribution spectra, a standard CONTIN_IT program was used, which is provided by the device developer.

One of the most important tasks in the study of productive deposits is to study the microstructures of the pore space of high-resolution core samples. Modern mathematical models of the pore space of rocks are performed with a fairly large share of assumptions and approximations, which actually translates them into the category of schemes. A qualitatively new level of study of reservoir rocks requires a modern approach to creating models.

Computer tomography provides detailed three-dimensional images of the internal structure of the rock without its destruction. CT data analysis allows to determine of the size, shape, and distribution of pores and other voids in

collecting rocks, as well as to evaluate filtration characteristics such as permeability and expulsion coefficient through mathematical modelling of physical processes. In this paper, CT is used to control changes in the shape of the pore space and the size of individual pores. The examination of samples with the CT method was carried out using the tomograph DeskTom 130 (France) equipped with a microfocus X-ray tube with a voltage of up to 150 kV and a focal spot size of up to 4 microns. The tomograph detector has a resolution of 1920 by 1536 pixels, with a physical size of 25 by 20 cm. The reconstruction was carried out using the "Xact" software. The results were analyzed in Avizo software. All the filming took place under the same conditions. During the filming, 1,440 two-dimensional shadow images were obtained for each sample at a voltage: 130 kV on an X-ray tube and a current of 61 mA. A 0.5 mm thick copper filter was used in the analysis. The survey resolution for the samples was 18.25 microns. Tomographic slices of one of the studied clayey limestone samples are presented in Figure 3.

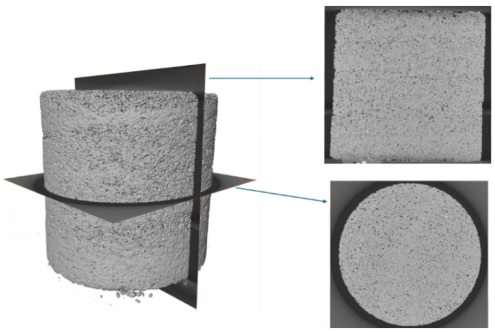

Figure 3. Tomographic slices of the studied clayey limestones

A distinctive feature of this work is the study of a method that combines laboratory X-ray CT and NMR. Pulsed nuclear magnetic resonance is one of the effective methods of laboratory studies of petrophysical characteristics of reservoir rocks. This method allows for obtaining qualitative and quantitative information about the structure of the pore space of the studied geological environment quickly and without mechanical impact.

The total porosity of the sample was determined by integrating the differential spectrum over the entire relaxation time interval. The components of the total porosity were determined by integrating the differential spectrum over petrophysical time intervals. The values of the time ranges of transverse relaxation-T2 for carbonate rocks were selected based on the average values of typical values for porosity components shown in Table 2.

The porosity coefficient of clays is the ratio of the volume of micropores to the volume of the rock. It mainly characterizes the porosity formed by the finely dispersed pelitic fraction (hydromica, smectites). It is advisable to assess clay content at residual saturation, when its influence is most significant [21, 22].

Table 2. Typical boundary values for porosity components [23]

Porosity Components	**Time Range of Change: Transverse Relaxation-T2**	
	T2 min, ms	**T2 max, ms**
Porosity of clays	0	3
Porosity filled by capillary-bound water	3	90 (carbonates) 33 (sandstones)
Porosity filled by irreducible water (displacement pressure, p = 0.7MPa)	0	90 (carbonates) 33 (sandstones)
Effective porosity (p = 0.7MPa)	90 (carbonates) 33 (sandstones)	The end value for the spectrum
Vuggy space (in carbonates)	750	The end value for the spectrum
Pore space (in carbonates)	0	750
Total porosity	0	The end value for the spectrum

3 Results and Discussion

As a result of evaluating the temporal variation of the amplitude of the NMR signal, it can be concluded that the average pore size after aging has become smaller. The red signal corresponds to limestone before exposure in the HMM, black-after (Figure 4).

The considered relaxation curve is a superposition of different relaxation time components, each of which corresponds to groups of pores of a certain size. NMR signal is proportional to the hydrogen content in the fluid contained in the porous media of the rock. Using calibration data, this signal can be converted into a porosity

coefficient. Assuming that pores are sufficiently large, hydrogen nuclei collide with pore walls less frequently. Hence, it takes magnetization a longer period of time to decrease, which leads to slower signal attenuation. Conversely, the signal from smaller pores decreases faster. Considering the intersection of two curves in Figure 4, it is difficult to determine if the pore size was greater before or after exposure in the HMM. However, the authors presume that the average pore size decreased after aging, given that for a long period of time, the NMR signal after aging was lower than before.

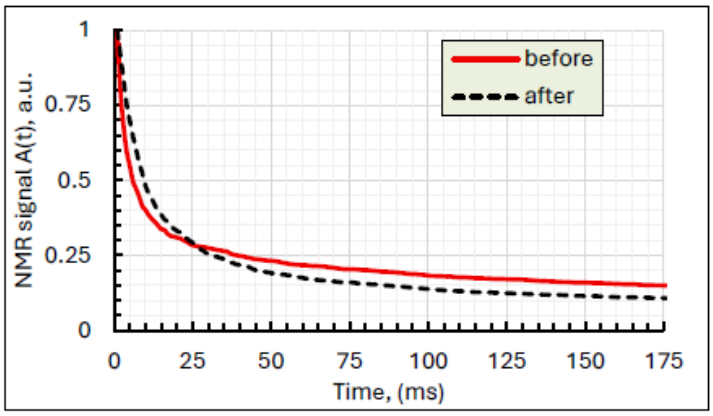

Figure 4. Before/After HMM relaxation curve

The differential spectrum characterizes the proportion of pores with a specific relaxation time T2 in the sample, and the integral spectrum is the change in porosity depending on the relaxation time (Figure 5). The graph shows the capillary and total porosity of the sample before/after exposure in HMM against the background of its integral spectrum. Using a 90 ms relaxation time cutoff for limestone, it is possible to estimate capillary porosity from the value of the integral spectrum at this point after deduction of the porosity of clays. The total porosity corresponds to the integral of the differential spectrum or the maximum of the integral spectrum. The effective porosity can be calculated as the value of a certain integral of the differential spectrum from 90 ms to the maximum relaxation time, or as the difference between the total and capillary porosity in the integral spectrum. The results presented in Figure 5 revealed that the porosity of clays that correspond to relaxation times lower than 3 ms became higher after exposure to HMM. Capillary porosity between 3 and 90 ms is higher after exposure as well. There is also a local maximum of porosity in this region that appeared after exposure. It may indicate the formation of a more complex capillary pore structure. Since relaxation times greater than 90 ms correspond to effective porosity, it can be concluded that effective porosity decreased after exposure to HMM. A local maximum is present in this region after exposure as well. It indicates a significant contribution from a specific pore size to overall and effective porosity.

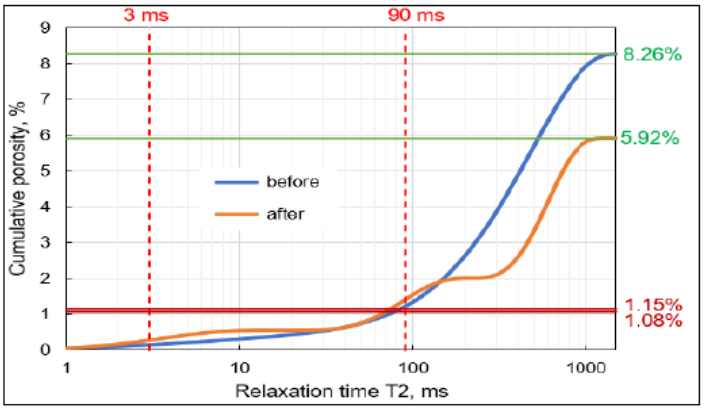

Figure 5. Integral spectrum of the sample before/after exposure in HMM

Table 3 shows the porosity components of the samples before and after exposure in the hydrogen-methane mixture, calculated from the results of NMR analysis. It corresponds to Figure 5 and the values marked on the graph. Considering the differential spectrum, one can see the presence of two local maxima before exposure and three after. Since the relaxation times correspond to certain pore sizes, and shorter times to smaller sizes, we can

assume an increase in the size of the main pore group and the appearance of an additional pore group of a certain size. Maxima of incremental porosity at small relaxation times represent small pores, such as clay and capillary pores. The greater value of the maximum incremental porosity correlates with an increase in capillary and clay porosity (Table 3, Figure 5). Beyond that, the maximum shifts toward intermediate-sized pores, as visible in the graph. Local maxima in the region of long relaxation times indicate larger pore groups. The small peak in this region split into two peaks after exposure in HMM, meaning that there are now two distinct large pore groups in the sample.

Table 3. Calculated porosity of samples before/after exposure in HMM based on NMR results

Sample Condition	Porosity of Clays, (%)	Capillary Porosity (%)	Effective Porosity (%)	Total Porosity (%)
Before	0.15	1.08	7.02	8.26
After	0.28	1.15	4.49	5.92

Analyzing the presented table, we can note a decrease in effective and total porosity and an increase in the values of capillary porosity and porosity of clays after exposure in HMM. Clayey limestones are facially associated with the overlying stratum of clay sandstones. Recalculation of NMR signals suggests that the sealing properties may be degraded due to the injection of HMMs, which may reduce their field characteristics. Figures 6-7 show the differential and integral spectra before and after exposure in the HMM. The red signal corresponds to the studied clayey limestone before the experiment, the black signal-after.

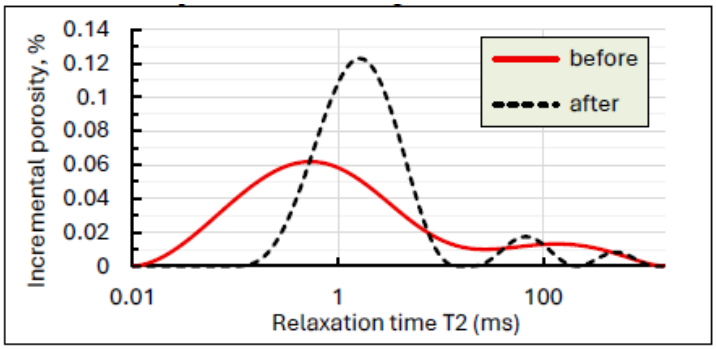

Figure 6. Spectral distribution over time of longitudinal relaxation T2

The three groups of pore sizes after exposure are clearly visible on the integral spectrum presented on a linear (non-logarithmic scale). Moreover, straight sections of the integral curve, especially on a linear scale, which do not contribute to the total porosity, as well as sections of the differential spectrum close to zero, show the appearance after aging of "degenerate" or "disappeared" pore sizes that were presented before aging, as shwon in Figure 7. Rapid accumulation of porosity after exposure to HMM indicates a significant contribution from pores within these relaxation time ranges, and consequently, within these pore size ranges. The more gradual increase before exposure suggests a more uniform pore distribution.

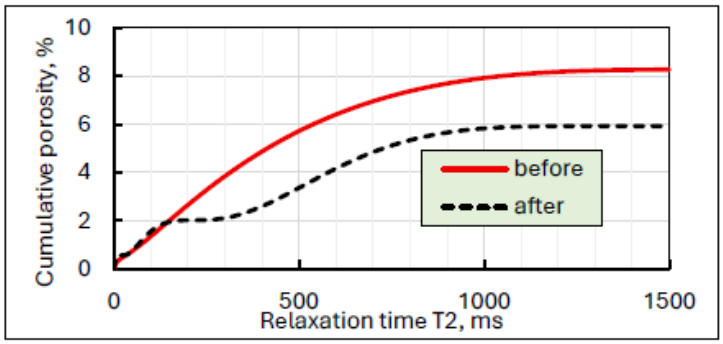

Figure 7. Cumulative porosity/integral spectrum before/after HMM

As a result of CT analysis processing, it was possible to build a model of the associated void space, as shown in Figure 8. Three-dimensional reconstruction of the pore spaces for the two samples studied was created by the results of computed tomography. Figure 8 illustrates sample 126-5, for which the following porosity characteristics were

determined before in HMM: total porosity was 6.7%, effective porosity was 6.1% After exposure in the specified gas environment, the indicators were 6.6% of total pore volume and 6.0% of effective porosity, respectively.

A similar model was created for sample 126-6, where the indicators of total and associated porosity were also revealed: 8.4% and 7.1%, respectively. After exposure in the gas mixture, the total porosity was 8.3%, and the associated porosity was 7.0%.

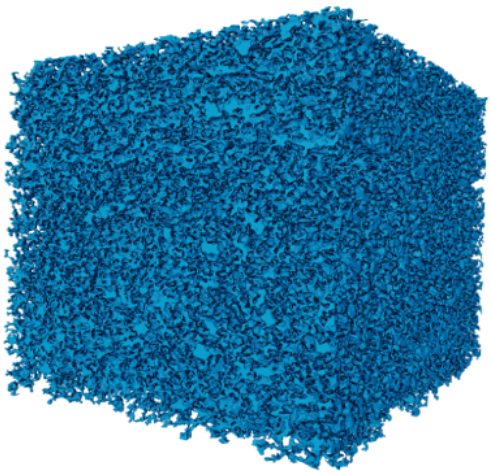

Figure 8. Model of the bound void space of the test sample based on CT results

Computed tomography obtained the following total and effective porosity values. White highlighted measurements for samples before exposure in the HMM, grey-after (Table 4).

Table 4. Calculated porosity of samples before/after exposure in HMM based on CT results

Sample Number	Effective Porosity, %	Total Porosity, %
126 − 5 before	6.1	6.7
126 − 5 after	6.0	6.6
126 − 6 before	7.1	8.4
126 − 6 after	7.0	8.3

CT also allowed analysis of the pore size distribution of the samples, as shown in Figures 9 and 10. This approach was previously described in the work of Al-Yaseri et al. [24].

Analysis of the samples showed that exposure in HMM led to a change in the pore size distribution in sample 126-5 as follows:

- The number of pores with diameters from 0.25–0.35 mm and from 0.4–0.5 mm increased.
- The pore sizes remained almost unchanged, ranging from 0.05–1 mm and from 0.2–0.25 mm, as well as exceeding 0.6 mm.
- The proportion of pores corresponding to diameter ranges from 0.1–0.2 mm, 0.3–0.4 mm, and 0.5–0.6 mm has decreased.
- Experimental data demonstrate that exposure of sample 126–6 in HMM resulted in the following pore size distribution.
- The number of pores with diameters between 0.1–0.25 mm and 0.3–0.35 mm has increased.
- The distribution of pores from 0.05 to 1 mm in size, as well as over 0.6 mm, remained unchanged.
- The observed decrease is typical for pores, the size of which corresponds to the ranges 0.25–0.3 mm, 0.35–0.45 mm, and 0.5–0.55 mm.

In this manner, despite the fact that there is some inconsistency between the NMR and CT results, the nature of changes after exposure in the hydrogen-methane mixture is similar—total porosity decreased after exposure. A possible reason for the differences is the fact that the NMR spectra correspond to the pore size distribution (the relaxation time is T2 related to the pore size), provided that the test rock is completely saturated with water (immersed in a container of water). Thus, if the water saturation is incomplete, it is possible to analyze the results only for pores filled with water. However, the general nature of the changes (porosity decreases after exposure in HMM) should not be affected, which can be traced from the results obtained in the framework of this work.

It is acceptable to compare pore size distributions obtained by CT and differential NMR spectra. Therefore, the spectral distribution over time of longitudinal relaxation T2 and pore size distribution (CT data) in sample 126-5

before/after exposure in HMM were analyzed (Figure 9 and Figure 10). The sample curve after exposure in HMM on the differential NMR spectrum should correspond to the bar graph of the distribution of CT pores in size after exposure in HMM. The sample curve before exposure in HMM on the NMR spectrum should correspond to the bar graph of pore size CT.

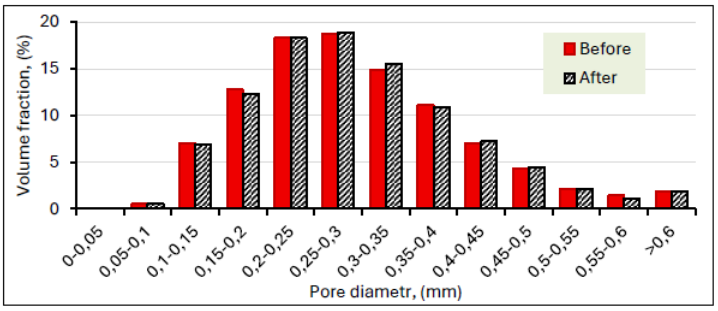

Figure 9. Pore size distribution by CT of sample 126-5 before/after exposure in HMM

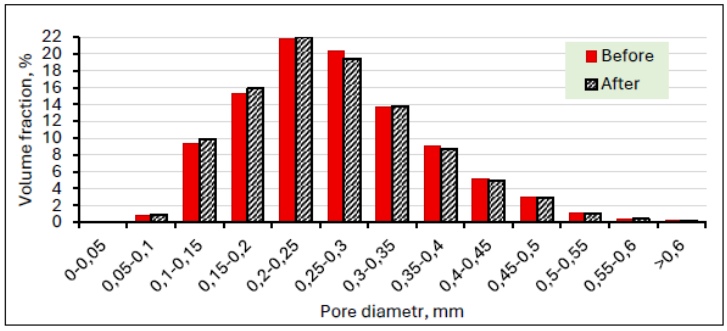

Figure 10. Pore size distribution by CT of sample 126-6 before/after exposure in HMM

A comparison was made of CT data, which, in the context of this study, appears to be a more reliable method for analyzing samples than NMR. From the point of view of the nature of changes in the sample after exposure in a hydrogen-methane mixture, the computed tomography data are consistent with the NMR data: the porosity of the samples, both total and effective, decreased after exposure. Considering the CT results, we can say that the changes associated with exposure in the hydrogen-methane mixture are insignificant—the decrease in porosity does not exceed a tenth of a percent. To assess the repeatability of NMR and CT results, the porosity of sample 126-5 was compared (Table 5).

Table 5. Calculated porosity of samples before/after exposure in HMM based on CT results

Sample Number	Total Porosity from NMR, %	Total Porosity from CT, %
Before	8.26	6.7
After	5.92	6.6

In general, by analyzing the pre- and post-exposure pore CT distributions, the changes associated with HMM exposure can be described as insignificant.

As a result of laboratory analyses using an IR spectrometer, IR spectra of crushed core samples were obtained (Figure 11). It was noted that, as a result, hydrogen was embedded into microcracks, edges, and screw dislocations.

On the spectra of the samples studied, a high peak in the absorption range of 700–850 cm^{-1} indicates a high percentage of both calcite and dolomite in the rock. A peak caused by out-of-plane bending vibration CO_3^{2-} was noted in the absorption band zone, tending to the values of 870–900 cm^{-1} [25]. Infrared absorption spectra of calcite and dolomite minerals are characterized by two absorption peaks with maxima at 887–897 cm^{-1} and 710–770 cm^{-1}, the second range is the most diagnostic characteristic and is used for both qualitative and quantitative determination of the rock mineral constitution. The amplitude of C-O bond deformation oscillations is caused by desorption of carbon dioxide (CO_2) from calcium carbonate ($CaCO_3$) and a decrease in the number of Si-O-Si crystalline quartz framework structures. The absorption range observed in the emissivity signals of samples in the spectral range of 900–1160 cm^{-1} corresponds to clay minerals (aluminosilicates).

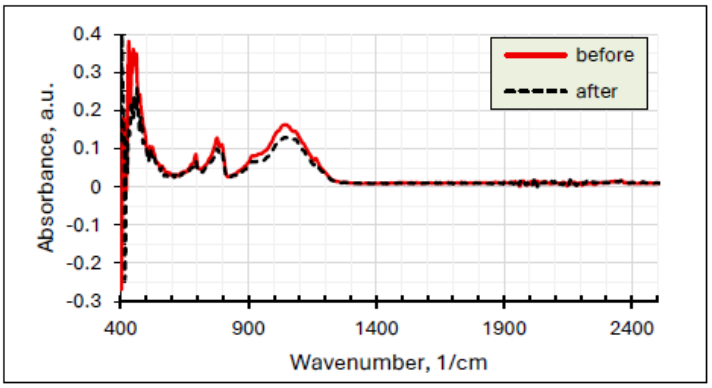

Figure 11. Infrared absorption spectra measurement results by Fourier IR spectroscopy of sample 126-6, which is taken from the original core sample and the exposed sample

At an absorption frequency of 1088 cm^{-1}, a wide absorption band is observed, which may be due to fluctuations in Si-O-Si bonds of the silica framework. A band of about 1,050–1,100 cm^{-1} is found in the spectra of rhombic carbonates and can serve as their diagnostic sign. However, the peak appearing in the region of 1000–1100 cm^{-1} can be due to both the absorption of carbonates and impurities, since silicates are strongly absorbed in this region. The Al-Al-OH deformation vibration band corresponds to the peak of 914 cm^{-1}, which is also reported by Udvardi et al. [26]. Such changes in the IR spectrum confirm the chemical bonding of hydrogen with mineral particles and organic compounds [27].

4 Conclusions

The combined use of CT and NMR methods demonstrated their complementarity in assessing changes in the pore structure of clayey limestones under the influence of HMM. CT provides more reliable data on the overall porosity structure, while NMR allows a more detailed analysis of the pore size distribution. The study revealed a slight decrease in total and effective porosity (by about 0.1%) after exposure in HMM, which indicates the stability of the main reservoir properties of the rock. A significant increase in clay porosity was noted (from 0.15% to 0.28%), which requires special attention to monitoring the state of clay strata and their sealing properties during long-term storage of HMM. The analysis of pore size distribution showed a decrease in the average pore size and the appearance of an additional group of pores after exposure in HMM. The results of IR spectroscopy confirmed the interaction of hydrogen with rock-forming minerals, including calcite and aluminosilicates, which is accompanied by changes in the mineral composition of the rock. The dissolution of calcite, from a geochemical point of view, causes clogging of pores, which limits the hydrodynamic flow of injected hydrogen in the tank. The mineral framework of limestones can be disturbed due to structural microdamage.

The obtained data indicate the need for further research into the long-term effects of HMM on the properties of carbonate rocks, especially in terms of maintaining the integrity of the reservoir and sealing complexes.

Summarizing all the above arguments, below are the key findings:

- After exposure in hydrogen, the pore size decreased, and an additional group of pore sizes was formed.
- After exposure, the total and effective porosity of the samples decreased.
- Capillary porosity and clay porosity have increased, which justifies the need to monitor the integrity of clay seals.

The study showed that a single injection of gas did not have a significant effect on the pore space. However, it requires further monitoring of the condition of rocks during prolonged exposure. The described results are useful in terms of understanding the structural stability of carbonate rocks when exposed to hydrogen, including together with methane.

As part of the expansion of research tasks on this topic, it is recommended to assess the reaction of hydrogen with carbonate minerals in order to reliably represent the degree of reactivity of hydrogen with carbonate rock.

Funding

The article was written within the framework of the budget assignment No. 125020501406-8 (FMME-2025-0011) on the topic "Geological substantiation of optimal conditions for natural and induced intra-reservoir revolution and its underground storage in depleted hydrocarbon deposits and salt structures".

Data Availability

The data used to support the research findings are available from the corresponding author upon request.

Conflicts of Interest

The authors declare no conflicts of interest.

References

[1] R. Tarkowski, "Underground hydrogen storage: Characteristics and prospects," *Renew. Sust. Energ. Rev.*, vol. 105, pp. 86–94, 2019. https://doi.org/10.1016/j.rser.2019.01.051

[2] A. Raza, M. Arif, G. Glatz, M. Mahmoud, M. Al Kobaisi, S. Alafnan, and S. Iglauer, "A holistic overview of underground hydrogen storage: Influencing factors, current understanding, and outlook," *Fuel*, vol. 330, p. 125636, 2022. https://doi.org/10.1016/j.fuel.2022.125636

[3] TNO, "Large-scale energy storage in salt caverns and depleted fields project findings," TNO, Tech. Rep. TNO 2020 R12006, 2020. https://publications.tno.nl/publication/34637700/8sBxDu/TNO

[4] L. A. Abukova, Y. A. Volozh, D. S. Filippova, and E. A. Safarova, "The search for natural hydrogen in Russia: State of the problem and possible starting solutions," *Dokl. Earth Sci.*, vol. 519, pp. 2063–2071, 2024. https://doi.org/10.1134/s1028334x24604012

[5] B. Hagemann, M. Rasoulzadeh, M. Panfilov, L. Ganzer, and V. Reitenbach, "Hydrogenization of underground storage of natural gas. Impact of hydrogen on the hydrodynamic and bio-chemical behavior," *Comput. Geosci.*, vol. 20, pp. 595–606, 2016. https://doi.org/10.1007/s10596-015-9515-6

[6] A. Rockson, F. Adesina, and F. Ian, "Geochemical stability of carbonate reservoirs for safe and efficient underground hydrogen storage: A case study in North Dakota's red river formation," in *SPE International Conference on Oilfield Chemistry*, Galveston, Texas, USA, 2025. https://doi.org/10.2118/224313-MS

[7] H. Galvis-Silva and E. R. Okoroafor, "Evaluating carbonate reservoir rocks for underground hydrogen storage: A comprehensive laboratory approach," in *SPE Annual Technical Conference and Exhibition*, New Orleans, Louisiana, USA, 2024. https://doi.org/10.2118/220971-MS

[8] A. E. Yekta, M. Pichavanta, and P. Audigane, "Evaluation of geochemical reactivity of hydrogen in sandstone: Application to geological storage," *Appl. Geochem.*, vol. 95, pp. 182–194, 2018. https://doi.org/10.1016/j.apgeochem.2018.05.021

[9] O. P. Abramova, D. S. Filippova, and E. A. Safarova, "Reliability of underground storage of hydrogen together with methane in terrigenous geological formations," *Act. Probl. Oil Gas*, vol. 4, no. 31, pp. 62–76, 2020. https://doi.org/10.29222/ipng.2078-5712.2020-31.art8

[10] L. Ganzer, V. Reitenbach, D. Pudlo, M. Panfilov, D. Albrecht, and R. Gaupp, "The H2STORE project—Experimental and numerical simulation approach to investigate processes in underground hydrogen reservoir storage," in *75th EAGE Conference & Exhibition incorporating SPE EUROPEC 2013*, London, UK, 2013. https://doi.org/10.3997/2214-4609.20130497

[11] V. Reitenbach, L. Ganzer, D. Albrecht, and B. Hagemann, "Influence of added hydrogen on underground gas storage: A review of key issues," *Environ. Earth Sci.*, vol. 73, pp. 6927–6937, 2015. https://doi.org/10.1007/s12665-015-4176-2

[12] M. Aslannezhad, M. Ali, A. Kalantariasl, M. Sayyafzadeh, Z. You, S. Iglauer, and A. Keshavarz, "A review of hydrogen/rock/brine interaction: Implications for hydrogen geo-storage," *Prog. Energy Combust. Sci.*, vol. 95, p. 101066, 2023. https://doi.org/10.1016/j.pecs.2022.101066

[13] S. Flesch, D. Pudlo, D. Albrecht, A. Jacob, and F. Enzmann, "Hydrogen underground storage—Petrographic and petrophysical variations in reservoir sandstones from laboratory experiments under simulated reservoir conditions," *Int. J. Hydrogen Energy*, vol. 10, pp. 1–14, 2018. https://doi.org/10.1016/j.ijhydene.2018.09.112

[14] H. Al-Mukainah, A. Al-Yaseri, N. Yekeen, J. Al Hamad, and M. Mahmoud, "Wettability of shale–brine–h2 system and h2-brine interfacial tension for assessment of the sealing capacities of shale formations during underground hydrogen storage," *Energy Rep.*, vol. 8, pp. 8830–8843, 2022. https://doi.org/10.1016/j.egyr.2022.07.004

[15] Y. Gogotsi, C. Portret, S. Osswald, J. M. Simmons, T. Yildirim, G. Laudisio, and J. Fischer, "Importance of pore size in high-pressure hydrogen storage by porous carbons," *Int. J. Hydrogen Energy*, vol. 34, no. 15, pp. 6314–6319, 2009. https://doi.org/10.1016/j.ijhydene.2009.05.073

[16] N. Heinemann, J. Alcalde, J. M. Miocic, S. J. T. Hangx, J. Kallmeyer, C. O. Henning, A. Hassanpouryouzband, E. A. Thaysen, G. J. Strobel, and C. e. a. Schmidt-Hattenberger, "Enabling large-scale hydrogen storage in porous media—The scientific challenges," *Energy Environ. Sci.*, vol. 14, no. 2, pp. 853–864, 2021. https://doi.org/10.1039/d0ee03536j

[17] C. Hemme and W. V. Berk, "Hydrogeochemical modeling to identify potential risks of underground hydrogen storage in depleted gas fields," *Appl. Sci.*, vol. 8, no. 11, p. 2282, 2018. https://doi.org/10.3390/app8112282

[18] A. Al-Yaseri and A. Fatah, "Impact of H2-CH4 mixture on pore structure of sandstone and limestone formations relevant to subsurface hydrogen storage," *Fuel*, vol. 358, p. 130192, 2024. https://doi.org/10.1016/j.fuel.2023.130192

[19] O. E. Aksyutin, A. G. Ishkov, K. V. Romanov, and R. V. Teterevlev, "Methane-hydrogen energy for low-emission development," *Gas Ind.*, vol. 11, pp. 120–125, 2018.

[20] A. G. Ishkov, N. B. Nesterov, K. V. Romanov, E. Koloshkin, S. Y. Nastich, V. Egorov, and V. Lopatkin, "Risks of using the gas transportation system for hydrogen energy," *Energy Policy*, vol. 193, pp. 56–67, 2024. http://doi.org/10.46920/24095516_2024_2193_56

[21] V. I. Galkin, O. A. Melkishev, and Y. V. Savitsky, "Statistical analysis of determining porosity factor of oil and gas reservoir rocks using gas volumetry and x-ray tomography methods," *Mining Sci. Technol.*, vol. 10, no. 3, pp. 221–231, 2025. https://doi.org/10.17073/2500-0632-2024-08-299

[22] L. R. Khanipova and Y. A. Gutorov, "On the prospects of using nuclear magnetic logging to study the filtration and capacity properties of complex reservoirs under the conditions of gazpromneft-nng," *Oil Gas Bus.*, vol. 1, no. 3, pp. 24–30, 2012.

[23] I. S. Jafarov, P. E. Syngaevsky, and S. F. Khafizov, *Application of the Nuclear Magnetic Resonance Method to Characterize the Composition and Distribution of Formation Fluids*. Moscow: Chemistry, 2002. https://www.libex.ru/detail/book103759.html

[24] G. R. Coates, L. Xiao, and M. G. Prammer, *NMR Logging, Principles and Applications*. Halliburton Energy Services, 2001. https://www.vista-clara.com/wp-content/uploads/2020/10/NMRLoggingPrinciples-10.1.1.206.319.pdf

[25] A. Al-Yaseri, H. Al Mukainah, N. P. Yekeen, and A. Al-Qazim, "Experimental investigation of hydrogen-carbonate reactions via computerized tomography: Implications for underground hydrogen storage," *Int. J. Hydrogen Energy*, vol. 48, 2022. https://doi.org/10.1016/j.ijhydene.2022.10.148

[26] B. Udvardi, I. J. Kovács, P. Kónya, M. Földvári, J. Füri, F. Budai, F. Falus, T. Fancsik, C. Szabó, Z. Szalai, and J. Mihály, "Application of attenuated total reflectance fourier transform infrared spectroscopy in the mineralogical study of a landslide area," *Sediment. Geol.*, vol. 313, pp. 1–14, 2014. https://doi.org/10.1016/j.sedgeo.2014.08.005

[27] S. N. Popov, S. E. Chernyshov, X. Wang, and L. Hou, "Hydrogen influence on transformation of terrigenous reservoir physical and mechanical properties," *Adv. Geo-Energy Res.*, vol. 13, no. 3, pp. 193–202, 2024. https://doi.org/10.46690/ager.2024.09.05

Nomenclature

Kp	Porosity
$\mathrm{Kp_{cl}}$	Clay porosity
$\mathrm{Kp_{cbw}}$	Capillary-bound water porosity
$\mathrm{Kp_{eff}}$	Effective porosity
T2	Time range of change in transverse relaxation

Abbreviations

Al	aluminum
$\mathrm{CaCO_3}$	calcium carbonate
$\mathrm{CH_4}$	methane
$\mathrm{CO_2}$	carbon dioxide
CT	computed tomography
HMM	hydrogen-methane mixtures
USH	Underground storage of hydrogen
$\mathrm{H_2}$	hydrogen
IR	infrared spectroscopy
NMR	nuclear magnetic resonance
O	oxygen
OH	hydroxyl radical
SEM	scanning electron microscope
Si	silicon